An Extended Range of Stable Flux Reconstruction Schemes on Quadrilaterals for Various Polynomial Bases

Will Trojak[1] · **Rob Watson**[3] · **Peter Vincent**[2]

© The Author(s) 2023

Abstract

An extended range of energy stable flux reconstruction schemes, developed using a summation-by-parts approach, is presented on quadrilateral elements for various sets of polynomial bases. For the maximal order bases, a new set of correction functions which result in stable schemes is found. However, for a range of orders it is shown that only a single correction function can be cast as a tensor-product. Subsequently, correction functions are identified using a generalised analytic framework that results in stable schemes for total order and approximate Euclidean order polynomial bases on quadrilaterals—which have not previously been explored in the context of flux reconstruction. It is shown that the approximate Euclidean order basis can provide similar numerical accuracy as the maximal order basis but with fewer points per element, and thus lower cost.

1 Introduction

The high-order flux reconstruction (FR) method of Huynh [15] is an efficient and versatile method for approximating the solution of time dependent partial differential equations. Many works have explored a range of the analytical characteristics of FR in one-dimension [2, 15, 21, 31–33], but fewer works have studied FR as it is applied to quadrilaterals. Two key works

✉ Will Trojak
w.trojak@ibm.com

1   IBM Research, The Hartree Centre, STFC Laboratory Sci-Tech Daresbury, Warrington WA4 4AD, UK

2   Department of Aeronautics, Imperial College London, South Kensington, London SW7 2AZ, UK

3   Aeronautical and Automotive Engineering, Loughborough University, Loughborough LE11 3TU, UK

which have explored quadrilaterals and the stability of the method when correction functions are formed of a tensor-product of one-dimensional corrections functions are Sheshadri and Jameson [22] and Cicchino and Nadarajah [10]. Also of note is the work of Grazia et al. [12], which studied the links between FR and nodal discontinuous Galerkin (DG) for tensor product formulations. In the work of Sheshadri and Jameson [22] a stability proof was provided using surface terms which are not reconcilable with the earlier analytical approaches of Vincent et al. [33] and Ranocha et al. [21]. In the original study by Huynh [15] and in the later work of Trojak et al. [28], the properties of the FR method were explored using Fourier analysis on quadrilaterals—and stark differences were observed in the numerical properties of the method when the correction function was changed. Again, both papers made use of a tensor-product of one-dimensional schemes. There are also many works using Fourier analysis to study DG approaches with tensor product formulations, so examples of which are Hes [14],Hu et al. [13], Roux et al. [19] and reference therein. In the context of implicit large eddy simulation (ILES) several works have studied the effect of correction function, these include [4, 9, 30]. In particular the work of Vermeire and Vincent [30] performed a large sweep over a set of tensor-product corrections functions and demonstrated the extent to which aliasing errors can be affected by the correction function. Similar results were found later by Cox et al. [11] when studying the difference between FR, DG, and spectral difference.

The definition of stable FR schemes on quadrilaterals has been entirely limited to these tensor-product schemes, whereas on triangles wide sets of stable FR schemes have been defined—notably the sets of Castonguay et al. [7] and of Williams et al. [36]. More recently, the summation-by-parts (SBP) methods have gained significant research attention due to their utility in the analysis of methods. Using the SBP framework, Ranocha et al. [21] was able to define an extended set of one-dimensional stable FR schemes. More recently still, Trojak and Vincent [27] have made use of this method to extend the set of stable FR schemes on triangles.

Within the literature on finite elements, it has been common across many applications for the approximation space on a quadrilateral elements to make use of a maximal order polynomial basis. For example, a first order maximal order basis would include the terms 1, x, y, and xy. This does fit naturally with the element, but other choices are also compatible. In two works, Trefethen [25, 26] explored the effect of using other bases when approximating functions, and showed that the so-called Euclidean basis often performs nearly as well as a maximal order basis, but at a lower computational cost. However, this work did overlook one advantageous aspect of the maximal order basis: on quadrilaterals it allows for operators to be decomposed to utilise the tensor product for improved computational efficiency Świrydowicz et al. [24], Trojak et al. [29].

In this work, we will make use of the SBP methods set out by Trojak et al. [27] to produce an extended range of stable FR methods on quadrilaterals with a maximal order polynomial basis. This SBP approach will then be generalised to produce analogous sets of stable schemes for alternative bases. With these sets of stable schemes defined, we will go on to investigate the isotropy of the different bases to determine the potential suitability of lower-cost bases. Consequently, this work is structured with the preliminaries given in Sect. 2 and the key requirements for stability and symmetry defined in Sect. 3. Then, in Sect. 4, an extended range of stable FR methods for the maximal order basis is presented and the stability of tensor-product constructions investigated. In Sects. refsec:quadspsto and 6, additional sets of stable FR schemes are defined on two alternative polynomial bases, namely the total order basis and an approximate Euclidean order basis. In Sect. 7, some numerical tests are presented for the three bases, and finally, in Sect. 8, various conclusions are drawn.

2 Preliminaries

2.1 Flux Reconstruction

The flux reconstruction (FR) scheme was first introduced by Huynh [15] and has been applied to several element topologies and to both advection and advection–diffusion systems [6, 16]. To give a brief introduction to the FR method here, we will consider the advection equation in one dimension:

$$\frac{\partial u}{\partial t} + \frac{\partial f}{\partial x} = 0, \quad \text{for} \quad u(x, t) : K \times \mathbb{R}_+ \mapsto \mathbb{R}, \quad \text{and} \quad f(u) : \mathbb{R} \mapsto \mathbb{R}. \quad (2.1)$$

The FR algorithm makes use of a sub-division of the domain K, such that $K = \bigcup_{i=1}^{N} K_i$ and $K_i \bigcap K_j = \emptyset$ for $i \neq j$. For each element two sets of points are considered: a set located on the boundary, ∂K, called the flux points; and a second set called solution points, both such that $\mathbf{x} \in K_i$. The number of solution points is equal to the number of polynomial bases in the approximation space, and the number of flux points is equal to the number of bases in the trace of the approximation space. In one dimension, with an approximation space $\mathbb{P}_k$, there are $k + 1$ solution points and 2 flux points. Lagrange polynomials for the solution and discontinuous flux can then be constructed. To enforce conservation, the discontinuous flux must be made continuous, and in FR the following procedure is used:

$$\frac{\partial f}{\partial x} \approx J_i^{-1} \left[\frac{\partial f_i^{\delta}}{\partial \xi} + (f_L^{\text{num}} - f_L^{\delta}) \frac{dh_L}{d\xi} + (f_R^{\text{num}} - f_R^{\delta}) \frac{dh_R}{d\xi} \right] \quad (2.2)$$

Here, J_i^{-1} is the inverse of the spatial Jacobian. This is used as it is more efficient for interpolation and differentiation operators to work in a reference domain $\hat{K}$ parameterised by ξ. Assuming affine elements, we can define the transformation $J_i : \hat{K} \mapsto K$. The last two terms on right-hand side of (2.2) are the corrections to the flux which ensure conservation. The terms f_L^{num} and f_R^{num} are common numerical fluxes at the left and right interfaces, respectively, and f_L^{δ} and f_R^{δ} are the interpolated discontinuous fluxes at the left and right interfaces. Finally, the functions h_L and h_R are the left and right correction functions, with the boundary conditions that they equal one at their respective interfaces, and zero at their opposite interfaces. More detail on the correction functions will be given in the subsequent sub-section.

Once the continuous gradient of the flux is approximated, the method of lines can be used with an integration method such as explicit Runge–Kutta, or a more complex implicit approach can be used, such as those in Wang and Yu [34]. For a more detailed introduction to the FR method, the works of Grazia et al. [12] and Abe et al. [1] are recommended, along with the references therein.

2.2 Correction Functions

Since the inception of the FR method [15], it has been observed that changing the correction function can have a noticeable effect on the scheme's numerical properties. The first continuous set of correction functions was introduced by [31], where a stability proof in one dimension was set out for all functions comprising the set. These functions, parameterised

by a single variable, c, have the definition:

$$h_L = \frac{(-1)^k}{2} \left(\psi_k - \frac{\eta_k \psi_{k-1} + \psi_{k+1}}{1 + \eta_k} \right), \tag{2.3a}$$

$$h_R = \frac{1}{2} \left(\psi_k + \frac{\eta_k \psi_{k-1} + \psi_{k+1}}{1 + \eta_k} \right), \tag{2.3b}$$

with the constants:

$$\eta_k(c) = \frac{c(2k+1)(a_k k!)}{2}, \quad a_k = \frac{(2k)!}{2^k (k!)^2}, \quad \forall\, c \in \{c \in \mathbb{R};\, -1 < \eta_k(c) < \infty\}. \tag{2.4}$$

Here, ψ_i is the ith order Legendre polynomial. To construct correction functions for hypercube elements such as quadrilaterals and hexahedrons, a tensor product construction of one dimensional functions has typically been used. However, for triangular elements [7] an analogous proof to that used in 1D was constructed, enabling stable correction functions to be found without a tensor product formulation.

An alternative methodology to define stable correction functions was introduced by Vincent et al. [33] and later formalised within the summation-by-parts (SBP) framework by Ranocha et al. [21]. These works only focused on one-dimensional schemes, but they showed the utility of the discrete SBP framework in defining stable schemes. To allow the definition of FR on quadrilaterals to be extended, we now introduce the SBP framework.

2.3 Summation-By-Parts

Before defining SBP in higher dimensions, consider the following definitions. Take the domain $K \subset \mathbb{R}^d$, and let u_i be an approximation to the exact function u in element K_i. The vector $\mathbf{u}_i$ can then be defined, which is the function u_i evaluated at N_s solution points $\mathbf{x}_i = \{\mathbf{x}_{i,j}\}_{i \leq N_s}$. If we then have the Lagrange polynomials in element K_i such that $l_j(\mathbf{x}_{i,k}) = \delta_{jk}$ and $u_i = \sum_{j=1}^{N_s} u_i(\mathbf{x}_{i,j}) l_j$, a mass matrix can be defined, with entries:

$$\mathbf{M}_{jk} = \int_K l_j(\mathbf{x}) l_k(\mathbf{x}) d\mathbf{x}. \tag{2.5}$$

For cardinal axes $x_1, x_2, \ldots$, we can also define the differentiation matrices such that:

$$\mathbf{D}_{x_1} \mathbf{u}_i = \sum_{j=1}^{N_s} u_i(\mathbf{x}_{i,j}) \frac{dl_j}{dx_1}, \quad \mathbf{D}_{x_2} \mathbf{u}_i = \sum_{j=1}^{N_s} u_i(\mathbf{x}_{i,j}) \frac{dl_j}{dx_2}, \quad \ldots \tag{2.6}$$

Using these operators we can then define summation-by-parts as a discrete analogy of integration-by-parts, with the following definition:

Definition 1 (Generalised Summation-By-Parts) Let $u \in C^1(K)$ and $U \in (c^1(K))^d$, such that for some nodal point set $\{\mathbf{x}_i\}_{i \leq N} \subset K$ we have $\mathbf{u}_i = u(\mathbf{x}_i)$ and $\mathbf{U}_i = U(\mathbf{x}_i)$, then a set of operators is said to satisfy the generalised SBP property if:

$$\mathbf{MD} + \mathbf{G}^T \hat{\mathbf{M}} = \mathbf{L}_{\partial K}^T \mathbf{W}_{\partial K} \mathbf{N} \hat{\mathbf{L}}_{\partial K}, \tag{2.7}$$

where we have the divergence and gradient operators as:

$$\mathbf{DU} = [\mathbf{D}_{x_1}, \mathbf{D}_{x_2}, \ldots] \mathbf{U} \approx \nabla \cdot U \quad \text{and} \quad \mathbf{Gu} = \begin{bmatrix} \mathbf{D}_{x_1} \\ \mathbf{D}_{x_2} \\ \vdots \end{bmatrix} \mathbf{u} \approx \nabla u. \tag{2.8}$$

Then defining the interpolation $\mathbf{L}_{\partial K} : K \mapsto \partial K$, and boundary mass matrix, $\mathbf{W}_{\partial K}$, such that:

$$\mathbf{u}_i^T \mathbf{L}_{\partial K} \mathbf{W}_{\partial K} \mathbf{N} \hat{\mathbf{L}}_{\partial K} \mathbf{U}_i = \int_{\partial K} u_i U_i \cdot \mathbf{n}_i \, \mathrm{d}s, \tag{2.9}$$

where $\mathbf{n}$ is a vector function of outwards facing normals at the surface, and $\mathbf{N}$ is a matrix of these normals at the flux points. Here, we use the notation for the Kronecker product with the identity of:

$$\hat{\mathbf{B}} = \mathbf{B} \otimes \mathbf{I}_d. \tag{2.10}$$

Remark 1 The definition of the mass matrix given in (2.5) fully integrates the basis, however in many applications a quadrature is used instead of explicitly calculating the mass matrix. From (2.7) it is clear that the mass matrix has to have sufficient accuracy to be able to accurately integrate $\mathbf{u}^T \mathbf{MDu}$, however for some quadratures this is not always possible. Using the works of Chan [8] and Trojak and Vincent [27], this problem can be remedied by using a second set of points which do possess sufficient strength. In the context of FR, this additional point set is only required during the operator construction.

With these operators established, the FR method in multiple dimensions can then be rewritten as:

$$\nabla \cdot \mathbf{F} \approx \mathbf{DF} + \mathbf{C} \left((\mathbf{n} \cdot \mathbf{F}^{\mathrm{num}}) - \mathbf{N} \hat{\mathbf{L}}_{\partial} \mathbf{F} \right), \tag{2.11}$$

where $\mathbf{N}$ is a matrix of outwards facing normals and $\mathbf{C}$ is the correction matrix. This matrix is the discrete analogue of the gradient of the correction function terms in (2.2).

In this work we will often work with the modal form of operators. This is due to their relative sparsity compared to the nodal form. Transformation between the modal and nodal representations is performed by the Vandermonde matrix, $\mathbf{V}$, as:

$$\mathbf{u} = \mathbf{V} \tilde{\mathbf{u}}, \tag{2.12}$$

where $\tilde{\mathbf{u}}$ is a vector of modal coefficients. An operator matrix, $\mathbf{B}$, is transformed to modal form with:

$$\tilde{\mathbf{B}} = \mathbf{V}^{-1} \mathbf{B} \mathbf{V}. \tag{2.13}$$

In this work, a tilde is used to denote a matrix or vector in the *modal* representation.

2.4 Polynomial Basis

A systematic way to define a polynomial basis can be achieved through the L_p norm of a vector of orders. This is the method used by Trefethen [25], and examples are shown diagrammatically in Fig. 1 for two dimensions, where $\mathbf{k}$ is a vector of the basis orders. For example, the basis $\psi_1(x)\psi(y)_2$ would have the vector $[1, 2]^T$, where ψ_i is an ith order Legendre polynomial. Shown in Fig. 1 are the modes required for a total order, Euclidean order, and maximal order basis—these three bases will form the focus of this work. As outlined in the introduction, on quadrilaterals, maximal order bases have been previously used almost exclusively. One reason for this is that it fits naturally with the element topology. For example, with four corner nodes, the spatial Jacobian can be defined fully in the $k = 1$ maximal order basis, *i.e* bases 1, x, y, and xy.

(a) Two-dimensional vector norms.   (b) Resulting bases for $k_{max} = 5$.
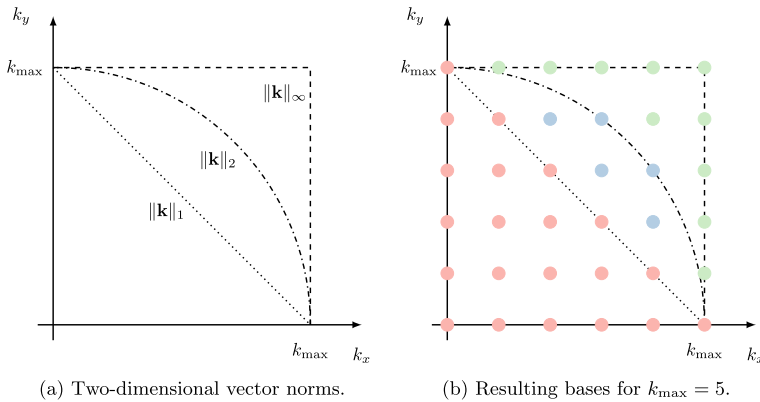
Fig. 1 Diagram of two-dimensional basis orders: total order $\|\mathbf{k}\|_1 \leq k_{max}$, Euclidean order $\|\mathbf{k}\|_2 \leq k_{max}$, and maximal order $\|\mathbf{k}\|_\infty \leq k_{max}$

Other basis functions can be chosen—such as rational functions or radial basis functions. However, except to address some specific deficiencies, these schemes are not widely used due to the additional computational complexities they add, with little benefit in the majority of cases [20, 35].

3 Linear Stability

In the works of Vincent et al. [33], Ranocha et al. [21], and Trojak and Vincent [27], the linear stability of flux reconstruction has been explored. The main result of those works is the following lemma for the linear stability of the FR method:

Lemma 1 (Linear Stability) *For flux reconstruction applied to (2.1) with* $\mathbf{f} = \mathbf{F} = \mathbf{a} \otimes \mathbf{u}$, *then satisfying the conditions that:*

$$\mathbf{Q} = \mathbf{Q}^T, \tag{3.1a}$$

$$(\mathbf{QD}) = -(\mathbf{QD})^T, \tag{3.1b}$$

$$\mathbf{v}^T(\mathbf{M} + \mathbf{Q})\mathbf{v} > 0, \tag{3.1c}$$

and

$$\mathbf{C} = (\mathbf{M} + \mathbf{Q})^{-1}\mathbf{L}_\partial^T \mathbf{W}_\partial, \tag{3.2}$$

with numerical flux such that:

$$(\mathbf{n} \cdot F)_j^{num+} = \frac{1}{2}(\mathbf{n}_j^+ \cdot \mathbf{a})(u_j^+ + u_j^-) - \frac{1}{2}\kappa|\mathbf{n}_j^+ \cdot \mathbf{a}|(u_j^- - u_j^+), \quad and \tag{3.3a}$$

$$(\mathbf{n} \cdot F)_j^{num-} = \frac{1}{2}(\mathbf{n}_j^- \cdot \mathbf{a})(u_j^- + u_j^+) - \frac{1}{2}\kappa|\mathbf{n}_j^- \cdot \mathbf{a}|(u_j^+ - u_j^-), \quad for \quad \kappa \in [0, 1], \tag{3.3b}$$

means the scheme is linearly stable, in that:

$$\frac{\mathrm{d}}{\mathrm{d}t}\|\mathbf{u}\|_{M+Q}^2 \leq 0. \tag{3.4}$$

Proof For a proof see Trojak and Vincent [27]. □

Fig. 2 Reference quadrilateral and the four face-relative coordinate systems

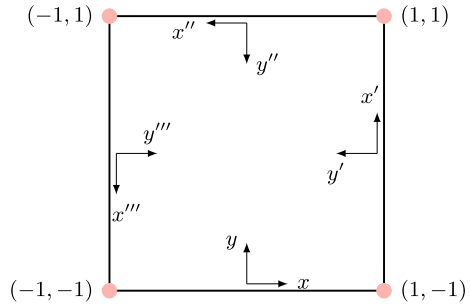The conditions set out in (3.1) and (3.2) allow for a parameterised $\mathbf{Q}$ that defines a continuous set of stable FR schemes to be found. The reduction of a generic $\mathbf{Q}$ matrix to enforce these conditions can be performed in a symbolic manipulation toolbox, and, by doing so, a general framework can be produced to find stable sets of FR schemes.

In addition to these conditions, it is assumed that the numerical properties of the method should be independent of the node ordering. Therefore, additional symmetry conditions are required for $\mathbf{Q}$ such that, for the four reference axes shown in Fig. 2, $\mathbf{Q}$ is independent of a particular frame of reference.

To achieve the desired symmetry properties, we first start by defining a transformation matrix from one reference frame to another, $\mathbf{T}$, and then enforce the following condition:

$$\tilde{\mathbf{T}}_{ab}\tilde{\mathbf{Q}} = \tilde{\mathbf{Q}}\tilde{\mathbf{T}}_{ab}, \tag{3.5}$$

here enforced in the modal representation. The matrix $\mathbf{T}_{ab}$ transforms a vector from reference frame a to frame b. In later sections, we will go on to explore alternative bases, for which rotationally symmetric point layouts are not possible. In these situations, a certain degree of anisotropy will have to be accepted, and at least with these symmetry conditions, the methods will be as symmetric as possible. Care should be taken when enforcing the symmetry conditions to not over-constrain $\mathbf{Q}$. For a quadrilateral, this means that only two rotations need to be enforced, as the remaining rotational and axial symmetries can be expressed in terms of just two rotations.

4 Extended-Range FR for Quadrilaterals

The overwhelming majority of polynomial finite element methods when applied to quadrilaterals use a maximal order basis, *i.e.* let@tokeneonedot$\|\mathbf{k}\|_\infty \leq k_{\max}$. To define an extended range of stable FR method in this case, the techniques of Sect. 3 can be applied. There are many possible options for the point sets. It has been shown that a tensor product of Gauss–Lobatto points is Fekete optimal [3], and that a tensor product of Chebyshev points is near optimal in a Lebesgue sense [5]. However, for methods such as FR, it is has been shown in one dimension that Gauss–Legendre points are optimal, and it has been suggested that this extends to higher dimensions via a tensor product [38].

The reference element for the quadrilateral used in this work is shown in Fig. 2, and the maximal order orthogonal basis is organised as:

$$\phi_i(x, y) = \psi_v(x)\psi_w(y), \quad \text{for} \quad i = w(k + 1) + v + 1, \quad \text{and} \quad 0 \leq v, w \leq k. \tag{4.1}$$

4.1 $k = 2$

Starting at $k = 2$, the conditions set out in Lemma 1 and the symmetry conditions can be enforced on a matrix, to find that applicable $\tilde{\mathbf{Q}}$ matrices have the form:

$$\tilde{\mathbf{Q}} = \begin{bmatrix} \mathbf{0} & & & & \mathbf{0} & & & \\ \mathbf{0} & 0 & 0\ 0\ 0 & & 0 & 0 & -3q_1 \\ & 0 & 0\ 0\ 0 & & 0 & 0 & 0 \\ & 0 & 0\ 0\ 0 & & 0 & 0 & 0 \\ & 0 & 0\ 0\ q_1 & & 0 & 0 & 0 \\ & 0 & 0\ 0\ 0 & & 0 & 0 & -3q_1 \\ & 0 & 0\ 0\ 0 & & 0 & q_1 & 0 \\ & -3q_1 & 0\ 0\ 0 & & -3q_1 & 0 & q_0 \end{bmatrix}. \tag{4.2}$$

For stability, it is required that $\tilde{\mathbf{M}} + \tilde{\mathbf{Q}}$ is positive definite in order to induce a valid norm. Therefore, this imposes some conditions on the values of $\tilde{\mathbf{Q}}$. These can be straightforwardly found via the Cholesky factorisation, and for $k = 2$ the conditions are:

$$q_1 > -4/15 \quad \text{and} \quad 50q_0 - 1125q_1^2 + 8 > 0. \tag{4.3}$$

4.2 $k = 3$

The analysis can be repeated for $k = 3$, to obtain:

$$\tilde{\mathbf{Q}} = \begin{bmatrix} \mathbf{0} & & & & & & \mathbf{0} & & & & & \\ \mathbf{0} & 0 & 0 & 0 & 0 & 0 & 0 & 0 & 0 & 0 & 0 & q_2 \\ & 0 & 0 & 0 & 0 & 0 & 0 & 0 & 0 & 0 & -3q_2/5 & 0 \\ & 0 & 0 & 0 & 0 & 0 & 0 & 0 & 0 & q_2 & 0 & -5q_1/3 \\ & 0 & 0 & 0 & 0 & 0 & 0 & 0 & 0 & 0 & 0 & 0 \\ & 0 & 0 & 0 & 0 & 0 & 0 & -3q_2/5 & 0 & 0 & 0 & 0 \\ & 0 & 0 & 0 & 0 & 0 & 9q_2/25 & 0 & 0 & 0 & 0 & 0 \\ & 0 & 0 & 0 & 0 & -3q_2/5 & 0 & q_1 & 0 & 0 & 0 & 0 \\ & 0 & 0 & 0 & 0 & 0 & 0 & 0 & 0 & 0 & 0 & 0 \\ & 0 & 0 & q_2 & 0 & 0 & 0 & 0 & 0 & 0 & 0 & -5q_1/3 \\ & 0 & -3q_2/5 & 0 & 0 & 0 & 0 & 0 & 0 & 0 & q_1 & 0 \\ & q_2 & 0 & -5q_1/3 & 0 & 0 & 0 & 0 & 0 & -5q_1/3 & 0 & q_0 \end{bmatrix} \tag{4.4}$$

for the conditions on stability that:

$$q_2^2 < \frac{16}{441}, \tag{4.5a}$$

$$-189q_2^2 + 140q_1 > -16, \tag{4.5b}$$

$$(4 - 21q_2)(1008q_2 + 2352q_0 + 12348q_2q_0 - 5292q_2^2 - 27783q_2^3$$
$$- 68600q_1^2 + 192) > 0. \tag{4.5c}$$

This procedure can be continued for any order, k, to recover the $\hat{\mathbf{Q}}$ matrix and stability conditions. The results for $k \geq 4$ are cumbersome and are therefore excluded for brevity and typesetting constraints.

4.3 Tensor-Product Schemes

In the earlier works on the topic of stable FR schemes for quadrilaterals, correction functions were constructed using a tensor product of stable one-dimensional schemes. We wish to understand if these tensor-product constructions can be found as a subset of the schemes defined here.

To do this we first consider the modal presentation of the one-dimensional class of Vincent et al. [31], which can be used to formulate a tensor-product modal correction matrix. For the case of $k = 2$ this leads to the $\tilde{\mathbf{C}}$ matrix:

$$\tilde{\mathbf{C}}_{tp} = \begin{bmatrix} 1/2 & 0 & 0 & 1/2 & 0 & 0 & 1/2 & 0 & 0 & 1/2 & 0 & 0 \\ 0 & 1/2 & 0 & 3/2 & 0 & 0 & 0 & -1/2 & 0 & -3/2 & 0 & 0 \\ 0 & 0 & 1/2 & \theta & 0 & 0 & 0 & 0 & 1/2 & \theta & 0 & 0 \\ -3/2 & 0 & 0 & 0 & 1/2 & 0 & 3/2 & 0 & 0 & 0 & -1/2 & 0 \\ 0 & -3/2 & 0 & 0 & 3/2 & 0 & 0 & -3/2 & 0 & 0 & 3/2 & 0 \\ 0 & 0 & -3/2 & 0 & \theta & 0 & 0 & 0 & 3/2 & 0 & -\theta & 0 \\ \theta & 0 & 0 & 0 & 0 & 1/2 & \theta & 0 & 0 & 0 & 0 & 1/2 \\ 0 & \theta & 0 & 0 & 0 & 3/2 & 0 & -\theta & 0 & 0 & 0 & -3/2 \\ 0 & 0 & \theta & 0 & 0 & \theta & 0 & 0 & \theta & 0 & 0 & \theta \end{bmatrix}, \quad (4.6)$$

for $\theta = 5/(45c + 2)$. Attempts can then be made to solve the following system to find a valid $\tilde{\mathbf{Q}}$:

$$\tilde{\mathbf{Q}}\tilde{\mathbf{C}}_{tp} = -\tilde{\mathbf{M}}(\tilde{\mathbf{C}}_{tp} - \tilde{\mathbf{C}}_{DG}), \quad (4.7)$$

where $\tilde{\mathbf{C}}_{DG}$ is the DG correction matrix, found from $\mathbf{C}_{DG} = \mathbf{M}^{-1}\mathbf{L}_\partial^T\mathbf{W}_\partial$. This substitution is used in (3.2) as it gives a simpler system to solve. Looking for solutions, only one is found: when $c = 0$ and $\tilde{\mathbf{Q}} = 0$.

Repeating this for analysis for the extended range of stable 1D FR schemes presented by Vincent et al. [33], we find the tensor-product modal correction matrix for $k = 2$ as:

$$\tilde{\mathbf{C}}_{tp} = \begin{bmatrix} -1/2 & 0 & 0 & 1/2 & 0 & 0 & 1/2 & 0 & 0 & -1/2 & 0 & 0 \\ 0 & -1/2 & 0 & -\theta_0 & 0 & 0 & 0 & -1/2 & 0 & -\theta_0 & 0 & 0 \\ 0 & 0 & -1/2 & \theta_1 & 0 & 0 & 0 & 0 & 1/2 & -\theta_1 & 0 & 0 \\ -\theta_0 & 0 & 0 & 0 & 1/2 & 0 & -\theta_0 & 0 & 0 & 0 & 1/2 & 0 \\ 0 & -\theta_0 & 0 & 0 & -\theta_0 & 0 & 0 & \theta_0 & 0 & 0 & \theta_0 & 0 \\ 0 & 0 & -\theta_0 & 0 & \theta_1 & 0 & 0 & 0 & -\theta_0 & 0 & \theta_1 & 0 \\ -\theta_1 & 0 & 0 & 0 & 0 & 1/2 & \theta_1 & 0 & 0 & 0 & 0 & -1/2 \\ 0 & -\theta_1 & 0 & 0 & 0 & -\theta_0 & 0 & -\theta_1 & 0 & 0 & 0 & -\theta_0 \\ 0 & 0 & -\theta_1 & 0 & 0 & \theta_1 & 0 & 0 & \theta_1 & 0 & 0 & -\theta_1 \end{bmatrix}, \quad (4.8)$$

with

$$\theta_0 = (63c_0 + 105c_1 + 18)/\Psi, \quad \Psi = 175c_1^2 - 42c_0 - 12, \quad \text{and} \theta_1 = 5/(5c_1 + 2). \quad (4.9)$$

Once more, solutions to the system shown in (4.7) can be sought, whereupon it is found that no solutions exist except for $c_0 = c_1 = 0$—the DG solution. This leads us to the following proposition: for quadrilateral elements, a correction matrix that is a tensor-product of a one-dimensional correction function is not a form of linearly stable filtered DG scheme—with the exception of DG itself—although norms can exist where monotonic decay is observed.

Table 1 Number of bases, n_b, for different norms in two dimensions

k_{max}	n_b		
	$\|\mathbf{k}\|_1$	$\|\mathbf{k}\|_2$	$\|\mathbf{k}\|_\infty$
1	3	3	4
2	6	6	9
3	10	11	16
4	15	17	25
5	21	26	36
6	28	35	49

(a) Point orbits for a quadrilateral, the eight point orbit is further parameterised by z.

(b) Padua points for $n = 3$ and the generating Lissajou curve.
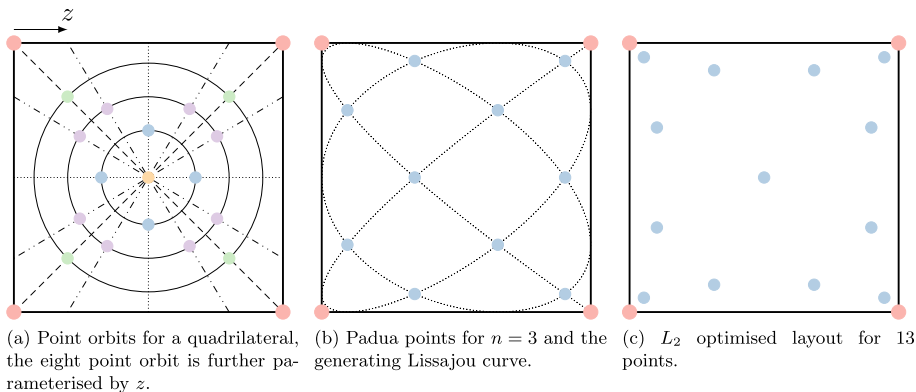
(c) L_2 optimised layout for 13 points.

Fig. 3 Various solution point layouts on the reference quadrilateral

5 Total Order Basis

Rather than the typical maximal order basis, if instead a total order basis is used, such that $\|\mathbf{k}\|_1 \leq k_{max}$, then a new set of stable FR schemes can be recovered. This basis is analogous to that used on triangular elements. A key requirement for finite element numerical methods is that the approximation space on the element boundary is the trace of the approximation space of the element. An advantage of hyper-cube topologies, such as the quadrilateral, is that it is trivial to show that for $\|\mathbf{k}\|_p \leq k_{max}$ this is true for $0 < p \leq \infty$.

For numerical methods that uses nodal values, a important characteristic for producing robust results is invariance of the numerical properties with node ordering. In flux reconstruction, requiring this invariance necessitates rotational symmetry of the solution and flux points and in the work of Witherden and Vincent [37] quadratures were found by enforcing this symmetry through orbit groups. For a square there are four such groups, and these groups are shown diagrammatically in Fig. 3a. However, from the number of basis functions for a given k_{max} shown in Table 1, it is apparent that the number of total order bases can not always be recovered using these orbits. For an example, consider $k_{max} = 2$—with six bases, the closest symmetric point layout would have five points.

One alternative to symmetric point layouts for total order are the Padua points [5], an example of which are shown in Fig. 3b. These points have several attractive properties: asymptotically they exhibit optimal growth of the Lebesgue measure on $[-1, 1]^2$ [5]; are unisolvent for arbitrary orders; and have $(n + 1)(n + 2)/2$ points, *i.e.*let@tokeneonedotthey

have the same number of points as a total order basis. However, they lack the full rotational symmetry of Fig. 3a.

With the total order basis introduced, we now enumerate some of the set of linearly stable FR methods on quadrilaterals with a total order basis.

5.1 $k = 2$

Starting with $k = 2$, enforcing the conditions on stability as presented in Lemma 1, we find that $\tilde{\mathbf{Q}}$ can have the form:

$$
\tilde{\mathbf{Q}} =
\begin{bmatrix}
0 & 0 & 0 & 0 & 0 & 0 \\
0 & 0 & 0 & 0 & 0 & 0 \\
0 & 0 & q_0 & 0 & 0 & q_2 \\
0 & 0 & 0 & 0 & 0 & 0 \\
0 & 0 & 0 & 0 & q_1 & 0 \\
0 & 0 & q_2 & 0 & 0 & q_0
\end{bmatrix}
\quad \text{for} \quad
\mathbf{\Phi}_2(x, y) =
\begin{bmatrix}
1 \\
\psi_0(x)\psi_1(y) \\
\psi_0(x)\psi_2(y) \\
\psi_1(x)\psi_0(y) \\
\psi_1(x)\psi_1(y) \\
\psi_2(x)\psi_0(y)
\end{bmatrix}
\tag{5.1}
$$

The condition of $\mathbf{M} + \mathbf{Q}$ being positive definite then leads to the conditions on stability that:

$$
q_1 > -4/9, \quad q_0 > -4/9, \quad \text{and} \quad (5q_0 + 4)^2 - 25q_2^2 > 0.
\tag{5.2}
$$

These conditions can be straightforwardly recovered from the condition that the Cholesky factorisation of a positive definite matrix has positive-real values on the leading diagonal.

5.2 $k = 3$

Repeating this process for $k = 3$:

$$
\tilde{\mathbf{Q}} =
\begin{bmatrix}
\mathbf{0} & & & \mathbf{0} & & & \\
\mathbf{0} & q_0 & 0 & 0 & 0 & 0 & q_2 & 0 \\
 & 0 & 0 & 0 & 0 & 0 & 0 & 0 \\
 & 0 & 0 & 0 & 0 & 0 & 0 & 0 \\
 & 0 & 0 & 0 & q_1 & 0 & 0 & q_2 \\
 & 0 & 0 & 0 & 0 & 0 & 0 & 0 \\
 & q_2 & 0 & 0 & 0 & 0 & q_1 & 0 \\
 & 0 & 0 & 0 & q_2 & 0 & 0 & q_0
\end{bmatrix}
\quad \text{for} \quad
\mathbf{\Phi}_3(x, y) =
\begin{bmatrix}
1 \\
\vdots \\
\psi_0(x)\psi_3(y) \\
\psi_1(x)\psi_0(y) \\
\psi_1(x)\psi_1(y) \\
\psi_1(x)\psi_2(y) \\
\psi_2(x)\psi_0(y) \\
\psi_2(x)\psi_1(y) \\
\psi_3(x)\psi_0(y)
\end{bmatrix}
\tag{5.3}
$$

subject to the conditions that:

$$
q_0 > -4/7, \quad q_1 > -4/15, \quad \text{and} \quad 28q_0 + 105q_0q_1 + 60q_1 - 105q_2^2 + 16 > 0.
\tag{5.4}
$$

As an example of the resulting correction field, Fig. 4 shows the $k = 3$ correction field for DG FR for two different flux points.

(a) First flux point $(-1, \frac{\sqrt{15+2\sqrt{30}}}{35})$.   (b) Second flux point $(-1, \frac{\sqrt{15-2\sqrt{30}}}{35})$.

Fig. 4 Divergence of DG correction field for $k = 3$ FR on a quadrilateral with total order basis for two flux points, shown in red

5.3 $k = 4$

By repeating the process again, the $\tilde{\mathbf{Q}}$ matrix and stability conditions have been found for $k = 4$:

$$
\tilde{\mathbf{Q}} =
\begin{bmatrix}
\mathbf{0} & & & & & \mathbf{0} \\
\mathbf{0} & q_0 & 0 & 0 & 0 & 0 & 0 & q_3 & 0 & 0 & q_5 \\
0 & 0 & 0 & 0 & 0 & 0 & 0 & 0 & 0 & 0 & 0 \\
0 & 0 & 0 & 0 & 0 & 0 & 0 & 0 & 0 & 0 & 0 \\
0 & 0 & 0 & 0 & 0 & 0 & 0 & 0 & 0 & 0 & 0 \\
0 & 0 & 0 & 0 & q_1 & 0 & 0 & 0 & 0 & q_4 & 0 \\
0 & 0 & 0 & 0 & 0 & 0 & 0 & 0 & 0 & 0 & 0 \\
0 & 0 & 0 & 0 & 0 & 0 & 0 & 0 & 0 & 0 & 0 \\
q_3 & 0 & 0 & 0 & 0 & 0 & 0 & q_2 & 0 & 0 & q_3 \\
0 & 0 & 0 & 0 & 0 & 0 & 0 & 0 & 0 & 0 & 0 \\
0 & 0 & 0 & 0 & q_4 & 0 & 0 & 0 & 0 & q_1 & 0 \\
q_5 & 0 & 0 & 0 & 0 & 0 & 0 & q_3 & 0 & 0 & q_0
\end{bmatrix}
\quad \text{for} \quad
\mathbf{\Phi}_4(x, y) =
\begin{bmatrix}
1 \\
\vdots \\
\psi_0(x)\psi_4(y) \\
\psi_1(x)\psi_0(y) \\
\psi_1(x)\psi_1(y) \\
\psi_1(x)\psi_2(y) \\
\psi_1(x)\psi_3(y) \\
\psi_2(x)\psi_0(y) \\
\psi_2(x)\psi_1(y) \\
\psi_2(x)\psi_2(y) \\
\psi_3(x)\psi_0(y) \\
\psi_3(x)\psi_1(y) \\
\psi_4(x)\psi_0(y)
\end{bmatrix}
\tag{5.5}
$$

subject to the constraints:

$$q_0 > -4/9, \tag{5.6a}$$

$$q_1 > -4/21, \tag{5.6b}$$

$$36q_0 + 225q_0q_2 + 100q_2 - 225q_3^2 + 16 > 0, \tag{5.6c}$$

$$(21q_1 + 4)^2 - 441q_4^2 > 0, \tag{5.6d}$$

Table 2 Approximate Euclidean basis p and n_b for various orders

k_{max}	2	3	4	5	6	7	8	9	10	11
p	48	50	2	21	3	3	2.2	2	2.4	2.2
n_b	8	13	17	29	37	45	60	73	92	109

$$(9q_0 - 9q_5 + 4)\left[9q_0(25q_2 + 4) + 25q_2(9q_5 + 4) + 2(-225q_3^2 + 18q_5 + 8)\right] > 0. \quad (5.6e)$$

6 Approximate Euclidean Order Basis

Across two works [25, 26], Trefethen investigated a Euclidean basis where $\|\mathbf{k}\|_2 \leq k_{max}$. In these works a paradox is pointed out: the total order basis is isotropic in the sense that the orders in various directions are equal, however the hyper-cube is exponentially anisotropic, and functions typically require higher orders along diagonals. The conclusion is that a truly isotropic basis for a hyper-cube is more similar to a Euclidean basis. However, as discussed in Sect. 1, maximal order bases have the computational advantage that operators can often be split to work along lines or by straightforwardly utilising there sparse structure. Alternatively, this sparsity will not be found with a Euclidean basis, however this will be ameliorated by fewer points per element. Finally, it is hypothesised that the additional resolution along the diagonal that is common to maximal order bases will only have a small impact on the error on convection dominated solutions, due to the movement of features and the already low impact on the error observed by Trefethen [25].

As discussed in Sect. 5, the symmetry orbits of a quadrilateral place a limit on the set of solution points. For a total order basis we can avoid this problem with the Padua points, as they are provably optimal in some respects; however, no analogous point set currently exists for a Euclidean basis. Therefore, a reasonable alternative is to increase the number of basis functions slightly so that they correspond to a number of points that can be found within the orbits of a quadrilateral. To do this, we can increase p in $\|\mathbf{k}\|_p \leq k_{max}$ until a symmetrical set of orbits can be found. This does not need to be performed with any great accuracy due to the discrete nature of the problem.

Table 2 shows the approximate values of p and n_b for various orders. We will call this basis an *approximate* Euclidean basis and we use the notation of $p = 2^*$ to indicate this. We now enumerate the resulting FR $\tilde{\mathbf{Q}}$ matrices and stability conditions for several of these orders.

6.1 $k = 2$

Unlike the true Euclidean order basis at $k = 2$, the approximate Euclidean basis has more points than the total order basis. We find that:

$$
\tilde{\mathbf{Q}} =
\begin{bmatrix}
0 & 0 & 0 & 0 & 0 & 0 & 0 & 0 \\
0 & 0 & 0 & 0 & 0 & 0 & 0 & -3q_1 \\
0 & 0 & 0 & 0 & 0 & 0 & 9q_1 & 0 \\
0 & 0 & 0 & 0 & 0 & -3q_1 & 0 & 0 \\
0 & 0 & 0 & 0 & q_1 & 0 & 0 & 0 \\
0 & 0 & 0 & -3q_1 & 0 & q_0 & 0 & 0 \\
0 & 0 & 9q_1 & 0 & 0 & 0 & 0 & 0 \\
0 & -3q_1 & 0 & 0 & 0 & 0 & 0 & q_0
\end{bmatrix},
\quad \text{for} \quad
\mathbf{\Phi}_2 =
\begin{bmatrix}
1 \\
\psi_0(x)\psi_1(y) \\
\psi_0(x)\psi_2(y) \\
\psi_1(x)\psi_0(y) \\
\psi_1(x)\psi_1(y) \\
\psi_1(x)\psi_2(y) \\
\psi_2(x)\psi_0(y) \\
\psi_2(x)\psi_1(y)
\end{bmatrix}. \tag{6.1}
$$

This is subject to the stability conditions stemming from positive definiteness and leads to the inequalities:

$$
60q_0 - 405q_1^2 > -16 \quad \text{and} \quad 2025q_1^2 < 16. \tag{6.2}
$$

6.2 $k = 3$

Repeating this for $k = 3$ we find:

$$
\tilde{\mathbf{Q}} =
\begin{bmatrix}
\mathbf{0} & & & & \mathbf{0} & \\
\mathbf{0} & q_0 & 0 & 0 & 0 & 0 & q_2 \\
& 0 & 0 & 0 & 0 & 0 & 0 \\
& 0 & 0 & 0 & 0 & 0 & 0 \\
& 0 & 0 & 0 & q_1 & 0 & 0 \\
& 0 & 0 & 0 & 0 & 0 & 0 \\
& q_2 & 0 & 0 & 0 & 0 & q_0
\end{bmatrix},
\quad \text{for} \quad
\mathbf{\Phi}_3 =
\begin{bmatrix}
1 \\
\vdots \\
\psi_1(x)\psi_3(y) \\
\psi_2(x)\psi_0(y) \\
\psi_2(x)\psi_1(y) \\
\psi_2(x)\psi_2(y) \\
\psi_3(x)\psi_0(y) \\
\psi_3(x)\psi_1(y)
\end{bmatrix}. \tag{6.3}
$$

which is subject to the stability conditions that:

$$
21q_0 > -4, \quad 25q_1 > -4, \quad \text{and} \quad 21q_0(21q_0 + 8) - 441q_2^2 > -16. \tag{6.4}
$$

An example of an approximate Euclidean order basis correction function is included in Fig. 5 for $\tilde{\mathbf{Q}} = 0$. Comparison with the correction function shown in Fig. 4 shows subtle differences, most notably in the ranges of the respective functions, which is shown more clearly in Fig. 8. A comparison of the Euclidean order basis DG correction function and the correction function for $\mathbf{Q}(q_0 = q_1 = q_2 = 1)$ are displayed in Fig. 9.

(a) First flux point $(-1, \frac{\sqrt{15+2\sqrt{30}}}{35})$.   (b) Second flux point $(-1, \frac{\sqrt{15-2\sqrt{30}}}{35})$.

Fig. 5 Divergence of DG correction field for $k = 3$ FR on a quadrilateral with an approximate Euclidean order basis for two flux points, shown in red

6.3 $k = 4$

We can repeat this analysis again for $k = 4$; however, in this case the approximate Euclidean order basis and the Euclidean order basis are the same. We then find that:

$$\tilde{\mathbf{Q}} = \begin{bmatrix} 0 & & & & & & & & 0 & & & & & \\ 0 & q_0 & 0 & 0 & 0 & 0 & 0 & 0 & 0 & 0 & 0 & 0 & 0 & q_3 \\ 0 & 0 & 0 & 0 & 0 & 0 & 0 & 0 & 0 & 0 & 0 & 0 & 0 & 0 \\ 0 & 0 & 0 & 0 & 0 & 0 & 0 & 0 & 0 & 0 & 0 & 0 & 0 & 0 \\ 0 & 0 & 0 & 0 & 0 & 0 & 0 & 0 & 0 & 0 & 0 & 0 & -5q_2/3 & 0 \\ 0 & 0 & 0 & 0 & 0 & 0 & 0 & 0 & 0 & 0 & 25q_2/9 & 0 & 0 \\ 0 & 0 & 0 & 0 & 0 & 0 & 0 & 0 & 0 & 0 & 0 & 0 & 0 & 0 \\ 0 & 0 & 0 & 0 & 0 & 0 & 0 & -5q_2/3 & 0 & 0 & 0 & 0 & 0 \\ 0 & 0 & 0 & 0 & 0 & 0 & 0 & q_2 & 0 & 0 & 0 & 0 & 0 \\ 0 & 0 & 0 & 0 & 0 & 0 & -5q_2/3 & 0 & q_1 & 0 & 0 & 0 & 0 \\ 0 & 0 & 0 & 0 & 0 & 0 & 0 & 0 & 0 & 0 & 0 & 0 & 0 \\ 0 & 0 & 0 & 0 & 25q_2/9 & 0 & 0 & 0 & 0 & 0 & 0 & 0 & 0 \\ 0 & 0 & 0 & -5q_2/3 & 0 & 0 & 0 & 0 & 0 & 0 & 0 & q_1 & 0 \\ q_3 & 0 & 0 & 0 & 0 & 0 & 0 & 0 & 0 & 0 & 0 & 0 & q_0 \end{bmatrix} \tag{6.5}$$

subject to the stability constraints that:

$$q_0 > -\frac{4}{9}, \tag{6.6a}$$

$$q_2 > -\frac{4}{25}, \tag{6.6b}$$

$$420q_1 + 48 - 4375q_2^2 > 0, \tag{6.6c}$$

$$144 - 30625q_2^2 > 0, \tag{6.6d}$$

$$9q_0(9q_0 + 8) - 81q_3^2 + 16 > 0. \tag{6.6e}$$

(a) Order of accuracy at $t = 20$. (b) Error for $N = 24^2$ at $t = 20$.

Fig. 6 Variation of order and error with angle, θ, for $k = 3$ DG FR with different bases

7 Numerical Experiments

In this section we present results of numerical experiments with the linear advection equation. In particular, we are concerned with:

$$\frac{\partial u}{\partial t} + \nabla \cdot \mathbf{a}u, \quad \text{for} \quad \mathbf{a} = \begin{bmatrix} \cos\theta \\ \sin\theta \end{bmatrix}. \tag{7.1}$$

To test the effects of anisotropy, we use a case comprised of several superimposed Morlet wavelets [18], with the definition:

$$u = c_\sigma \pi^{-1/4} \sum_{i=1}^{n} \exp(-r_i^2/2)\left[\cos(\sigma r_i) - \kappa_i\right], \tag{7.2a}$$

$$c_\sigma = \left[1 + \exp(-\sigma^2) - 2\exp(-3\sigma^2/4)\right]^{-1/2}, \tag{7.2b}$$

$$r_i = \sqrt{(x - x_i)^2 + (y - y_i)^2}, \tag{7.2c}$$

where (x_i, y_i) is a random centre coordinate, and σ and κ_i are control parameters. For the experiments conducted, four wavelets were superimposed, $n = 4$, with the control parameter σ set to three and $\kappa_i \in [0, 1]$ randomly chosen for each wavelet. In order to control for differing interpolation strength of this non-polynomial initial condition, a further projection set was taken. The initial condition was set via an L_2 projection of (7.2) on to the weakest total-order basis, this projected solution could then be interpolated onto the various point sets, ensuring the three bases have the same initial condition modally. This initial condition is ideal for testing isotropy due to the dependence on radius and wider frequency spectrum.

The domain used was fully periodic and covered $K \in [0, 2\pi]^2$, partitioned into N regular quadrilaterals. For time integration an explicit SSP-RK3 scheme was used with constant $\Delta t = 10^{-3}$, and for all tests the common interfaces were fully upwinded.

Initially, a sweep of advection angles for $N \in \{8^2, 10^2, \dots, 24^2\}$ was performed, the results of which are presented in Fig. 6. This shows a marked difference between the total order, approximate Euclidean order ($p = 2^*$), and maximal order bases. Most notably, the error when using a total order basis is significantly higher. This is consistent with the findings of Trefethen [25] for the interpolation error of the two-dimensional Runge function.
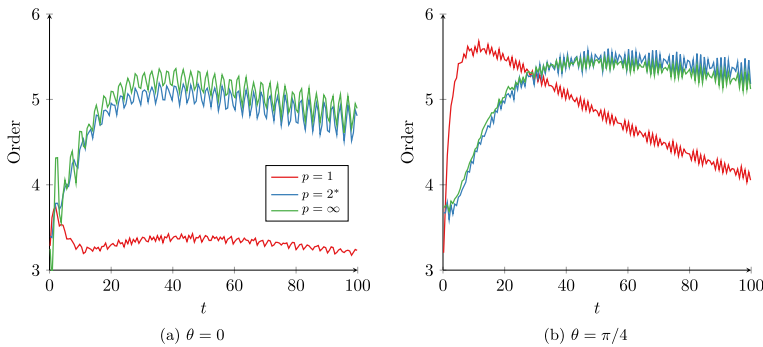
Fig. 7 Order versus time for $k = 3$ DG FR with different bases, calculated for $N = \{8^2, 12^2\}$

From Fig. 6a, we see that the order of accuracy of the total order scheme is higher for a large range of angles. Investigating this further, we present the variation of order in time calculated for two grids ($N \in \{8^2, 12^2\}$) and two angles, see Fig. 7. This shows that for non-grid aligned angles, the decay of the low order secondary modes is faster, seen by the faster transition from order $k + 1$ to $2k$. This is responsible for the apparently higher order shown in Fig. 6a. However, after the peak order of $2k$ is reached [2], the decay towards order $k + 1$, is faster and is generally indicative of the total order basis having larger dispersion and diffusion errors at higher frequencies. Decay in the order is seen for all bases as time progresses, and is due to dispersion errors at high frequencies. A further effect of the total order basis is observed in Fig. 7a, where for grid aligned waves the total order basis does not exhibit the super-convergence property observed for the other bases. From Fig. 6b, some asymmetry was observed in the total order basis error about $\theta = \pi/4$. As the basis itself is symmetric about $\theta = 45°$, this asymmetry is thought to be caused by a lack of full rational symmetry of the Padua points, as can be seen in Fig. 3b.

The points used for the $p = 2^*$ cases were optimised to reduce L_2 error, the result of which are shown Fig. 3c. Previously, it has been shown that use of L_2 optimal points are important in one dimension [37], yet closed forms for L_2 optimal points in higher dimension have been illusive. Instead, for the work here, a numerical optimisation was carried out on the symmetry orbits of the points, producing symmetrical sets of points which were distributed over the domain in such a way as to minimise a cost function. The cost function used was based on the L_2 norm of the ability of the interpolation of values at the solution points to approximate the behaviour of a large number of orthonormal polynomial bases computed over the cell. As alternatives to this novel approach, Lebesgue and Fekete optimal point sets were also produced—the results of which are not shown here, but which were significantly worse than those with L_2 optimised points in terms of absolute error.

The initial conditions used in this first batch of tests was set using the pointwise values of (7.2). Therefore the error displayed in Figs. 7 and 6 displays both the numerical error of the method and, when evaluated in the L_2 norm, the initial projection error. Therefore, to test the effect of this error a series of test was carried where the initial condition was projected to the respective bases via an L_2 projection operator constructed using a $(3k + 1)^2$ point Gauss–Legendre quadrature.

8 Conclusions

Three sets of linearly stable high-order flux reconstruction schemes on quadrilateral elements have been presented. These three sets were formed for the maximal order, total order, and

approximate Euclidean order polynomial bases. For the maximal order bases, it has been shown that the previously used tensor product of one-dimensional correction functions do not form part of this set, except for the DG correction functions themselves. Through numerical experimentation with the different bases, it was shown that the Euclidean order basis had similar performance to the maximal order basis, despite using fewer points, and was also significantly more isotropic than the total order basis. This result is consistent with previous observations made when using similar bases for polynomial interpolation. These methods can be applied to non-linear grid transformations in a free-stream preserving manner, similar to existing FR approaches, by using methods detailed in [1, 17]. Problems related to flux function aliasing can be tackled with several approaches, for example over-integration [23]. Future work will go on to investigate the utility of Euclidean basis polynomials in FR for real world non-linear problems.

Data Availability The data that support the findings of this study are available from the corresponding author upon reasonable request.

Declaration

Conflict of interest The authors have no relevant financial or non-financial interests to disclose.

A. Additional Correction Function Figures

Additional figures comparing correction functions.

(a) Approximate Euclidean order basis   (b) Total order basis
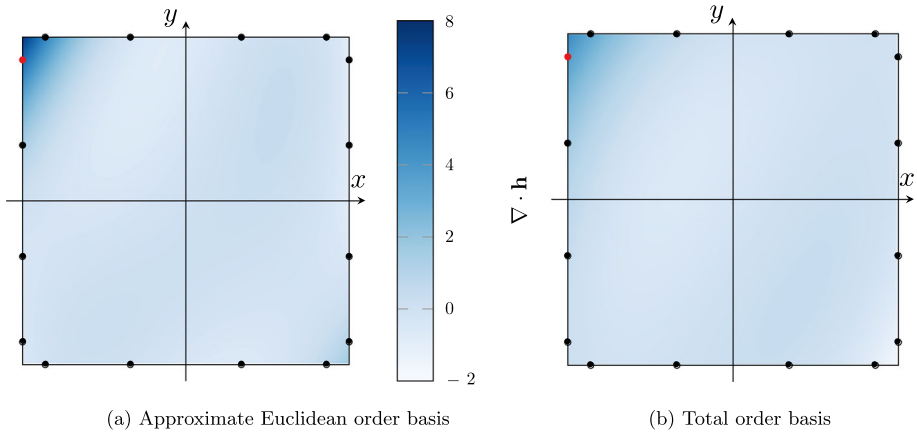
Fig. 8 Divergence of DG correction field for $k = 3$ FR on a quadrilateral with different bases for a flux point at $(-1, \frac{\sqrt{15+2\sqrt{30}}}{35})$, shown in red
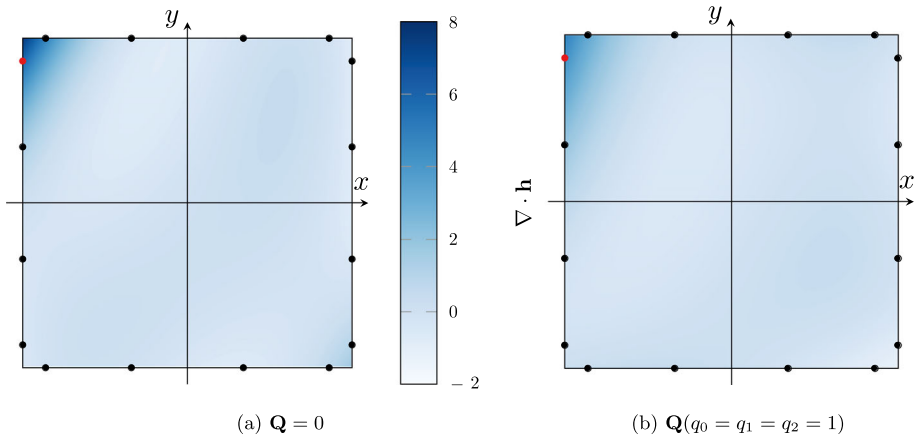

(a) $\mathbf{Q} = 0$ (b) $\mathbf{Q}(q_0 = q_1 = q_2 = 1)$

Fig. 9 Divergence of DG correction field for $k = 3$ FR on a quadrilateral with Euclidean order basis for a flux point at $(-1, \frac{\sqrt{15+2\sqrt{30}}}{35})$, shown in red, with two different $\mathbf{Q}$ matrices

References

1. Abe, Y., Haga, T., Nonomura, T., Fujii, K.: On the freestream preservation of high-order conservative flux-reconstruction schemes. J. Comput. Phys. **281**, 28–54 (2015). https://doi.org/10.1016/j.jcp.2014.10.011
2. Asthana, K., Watkins, J., Jameson, A.: On consistency and rate of convergence of flux reconstruction for time-dependent problems. J. Comput. Phys. **334**, 367–391 (2017). https://doi.org/10.1016/j.jcp.2017.01.008
3. Bos, L., Taylor, M.A., Wingate, B.A.: Tensor product Gauss–Lobatto points are Fekete points for the cube. Math. Comput. **70**(236), 1543–1547 (2001)
4. Bull, J.R., Jameson, A.: Simulation of the compressible Taylor green vortex using high-order flux reconstruction schemes. In: 7th AIAA Theoretical Fluid Mechanics Conference. American Institute of Aeronautics and Astronautics (2014). https://doi.org/10.2514/6.2014-3210
5. Caliari, M., De Marchi, S., Vianello, M.: Bivariate polynomial interpolation on the square at new nodal sets. Appl. Math. Comput. **165**(2), 261–274 (2005). https://doi.org/10.1016/j.amc.2004.07.001

6. Castonguay, P.: High-Order Energy Stable Flux Reconstruction Schemes For Fluid Flow Simulations on Unstructured Grids. PhD thesis, Stanford University, 5 (2012)

7. Castonguay, P., Vincent, P.E., Jameson, A.: A new class of high-order energy stable flux reconstruction schemes for triangular elements. J. Sci. Comput. **51**(1), 224–256 (2011). https://doi.org/10.1007/s10915-011-9505-3

8. Chan, J.: On discretely entropy conservative and entropy stable discontinuous Galerkin methods. J. Comput. Phys. **362**, 346–374 (2018). https://doi.org/10.1016/j.jcp.2018.02.033

9. Chen, L., Zhou, Z., Xia, J.: One-parameter optimal flux reconstruction schemes for adaptive mesh refinement. AIAA J. **60**(3), 1440–1450 (2022). https://doi.org/10.2514/1.j060856

10. Cicchino, A., Nadarajah, S.: A new norm and stability condition for tensor product flux reconstruction schemes. J. Comput. Phys. **429**, 110025 (2021). https://doi.org/10.1016/j.jcp.2020.110025

11. Cox, C., Trojak, W., Dzanic, T., Witherden, F.D., Jameson, A.: Accuracy, stability, and performance comparison between the spectral difference and flux reconstruction schemes. Comput. Fluids **221**, 104922 (2021). https://doi.org/10.1016/j.compfluid.2021.104922

12. De Grazia, D., Mengaldo, G., Moxey, D., Vincent, P.E., Sherwin, S.J.: Connections between the discontinuous Galerkin method and high-order flux reconstruction schemes. Int. J. Numer. Meth. Fluids **75**(12), 860–877 (2014). https://doi.org/10.1002/fld.3915

13. Hesthaven, J. S., Warburton, T.: Beyond One Dimension, chapter 6, pp 169–241. Springer, New York (2008). https://doi.org/10.1007/978-0-387-72067-8_6

14. Hu, F.Q., Hussaini, M.Y., Rasetarinera, P.: An analysis of the discontinuous Galerkin method for wave propagation problems. J. Comput. Phys. **151**(2), 921–946 (1999). https://doi.org/10.1006/jcph.1999.6227

15. Huynh, H.T.: A flux reconstruction approach to high-order schemes including discontinuous Galerkin methods. In: 18th AIAA Computational Fluid Dynamics Conference. American Institute of Aeronautics and Astronautics (2007). https://doi.org/10.2514/6.2007-4079

16. Huynh, H.T.: A reconstruction approach to high-order schemes including discontinuous Galerkin for diffusion. In: 47th AIAA Aerospace Sciences Meeting including The New Horizons Forum and Aerospace Exposition. American Institute of Aeronautics and Astronautics (2009). https://doi.org/10.2514/6.2009-403

17. Kopriva, D.A., Kolias, J.H.: A conservative staggered-grid Chebyshev multidomain method for compressible flows. J. Comput. Phys. **125**(1), 244–261 (1996). https://doi.org/10.1006/jcph.1996.0091

18. Kronland-Martinet, R., Morlet, J., Grossmann, A.: Analysis of sound patterns through wavelet transforms. Int. J. Pattern Recognit. Artif. Intell. **01**(02), 273–302 (1987). https://doi.org/10.1142/s0218001487000205

19. Le Roux, D.Y., Eldred, C., Taylor, M.A.: Fourier analyses of high-order continuous and discontinuous Galerkin methods. SIAM J. Numer. Anal. **58**(3), 1845–1866 (2020). https://doi.org/10.1137/19m1289595

20. Powell, M.J.D.: Rational approximation by the exchange algorithm. In: Approximation Theory and Methods, 1st ed., chapter 10, pp. 111–122. Cambridge University Press (1981). https://doi.org/10.1017/cbo9781139171502.011

21. Ranocha, H., Öffner, P., Sonar, T.: Summation-by-parts operators for correction procedure via reconstruction. J. Comput. Phys. **311**, 299–328 (2016). https://doi.org/10.1016/j.jcp.2016.02.009

22. Sheshadri, A., Jameson, A.: On the stability of the flux reconstruction schemes on quadrilateral elements for the linear advection equation. J. Sci. Comput. **67**(2), 769–790 (2015). https://doi.org/10.1007/s10915-015-0102-8

23. Spiegel, S.C., Huynh, H.T., DeBonis, J.R.: De-aliasing through over-integration applied to the flux reconstruction and discontinuous Galerkin methods. In: 22nd AIAA Computational Fluid Dynamics Conference. American Institute of Aeronautics and Astronautics (2015). https://doi.org/10.2514/6.2015-2744

24. Świrydowicz, K., Chalmers, N., Karakus, A., Warburton, T.: Acceleration of tensor-product operations for high-order finite element methods. Int. J. High Perform. Comput. Appl. **33**(4), 735–757 (2019). https://doi.org/10.1177/1094342018816368

25. Trefethen, L.N.: Multivariate polynomial approximation in the hypercube. Proc. Am. Math. Soc. **145**(11), 4837–4844 (2017). https://doi.org/10.1090/proc/13623

26. Trefethen, L.N.: Cubature, approximation, and isotropy in the hypercube. SIAM Rev. **59**(3), 469–491 (2017). https://doi.org/10.1137/16m1066312

27. Trojak, W., Vincent, P.: An Extended Range of Energy Stable Flux Reconstruction Methods on Triangles (2022)

28. Trojak, W., Watson, R., Scillitoe, A., Tucker, P.G.: Effect of mesh quality on flux reconstruction in multi-dimensions. J. Sci. Comput. **82**(3), 1 (2020). https://doi.org/10.1007/s10915-020-01184-2

29. Trojak, W., Watson, R., Witherden, F.D.: Hyperbolic diffusion in flux reconstruction: optimisation through kernel fusion within tensor-product elements. Comput. Phys. Commun. **273**, 108235 (2022). https://doi.org/10.1016/j.cpc.2021.108235
30. Vermeire, B.C., Vincent, P.E.: On the properties of energy stable flux reconstruction schemes for implicit large eddy simulation. J. Comput. Phys. **327**, 368–388 (2016). https://doi.org/10.1016/j.jcp.2016.09.034
31. Vincent, P.E., Castonguay, P., Jameson, A.: A new class of high-order energy stable flux reconstruction schemes. J. Sci. Comput. **47**(1), 50–72 (2010). https://doi.org/10.1007/s10915-010-9420-z
32. Vincent, P.E., Castonguay, P., Jameson, A.: Insights from von Neumann analysis of high-order flux reconstruction schemes. J. Comput. Phys. **230**(22), 8134–8154 (2011). https://doi.org/10.1016/j.jcp.2011.07.013
33. Vincent, P.E., Farrington, A.M., Witherden, F.D., Jameson, A.: An extended range of stable-symmetric-conservative flux reconstruction correction functions. Comput. Methods Appl. Mech. Eng. **296**, 248–272 (2015). https://doi.org/10.1016/j.cma.2015.07.023
34. Wang, L., Yu, M.: Comparison of ROW, ESDIRK, and BDF2 for unsteady flows with the high-order flux reconstruction formulation. J. Sci. Comput. **83**(2), 1 (2020). https://doi.org/10.1007/s10915-020-01222-z
35. Watson, R., Trojak, W.: On the Use of RBF Interpolation for Flux Reconstruction (2022)
36. Williams, D.M., Castonguay, P., Vincent, P.E., Jameson, A.: Energy stable flux reconstruction schemes for advection-diffusion problems on triangles. J. Comput. Phys. **250**, 53–76 (2013). https://doi.org/10.1016/j.jcp.2013.05.007
37. Witherden, F.D., Vincent, P.E.: On the identification of symmetric quadrature rules for finite element methods. Comput. Math. Appl. **69**(10), 1232–1241 (2015). https://doi.org/10.1016/j.camwa.2015.03.017
38. Witherden, F.D., Vincent, P.E.: On nodal point sets for flux reconstruction. J. Comput. Appl. Math. **381**, 113014 (2021). https://doi.org/10.1016/j.cam.2020.113014